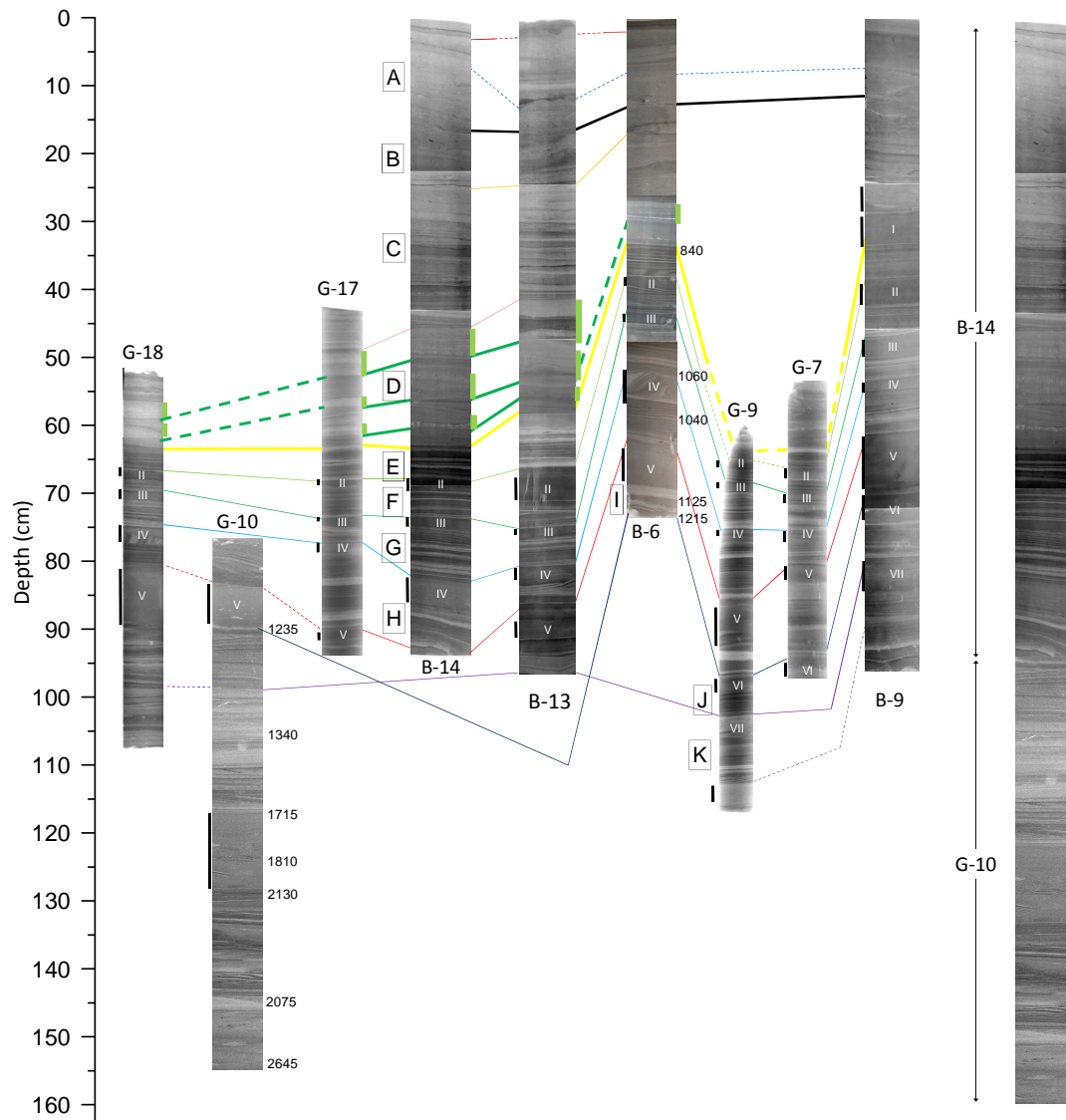


The response of the Peruvian Upwelling Ecosystem to centennial-scale global change during the last two millennia

SUPPLEMENTARY MATERIAL (SALVATTECI ET AL.)

SM1 (Figure):



SM 1. Cross correlation of laminated sequences among gravity cores (G) and box-cores (B). All the cores were retrieved off Pisco, Peru. The yellow lines indicate the position of the sedimentological shift (Gutierrez et al. 2009), the upper black bold lines indicate the start of ^{241}Am activities and the green thick lines indicate the correlations of the diatom-rich layers. The stratigraphic markers are represented by the continuous (dashed) colored thin lines that indicate possible (less obvious) correlations and represent the base of the sediment sequences (from A to K) except for the sections A and D where the base is

defined by the limit of detection of ^{241}Am and the sedimentary shift respectively. The capital letters from A to K indicate the position of contemporaneous sediment sequences. Black bars at the left side of the cores indicate homogeneous deposits, while green bars at the right side indicate the extent of the diatom layers. Given that the box-cores recovered surface sediments they are aligned at 0 cm; in contrast the gravity cores are aligned to the position of the shift in core B-14. In all the X-ray and SCOPIX images the colors were inverted, thus the darker (lighter) laminae represent dense (less dense) sediments. The numbers at the right side of the X-rays represent the uncalibrated ^{14}C ages. The composite record shown at the right side is the one used for the present study. Figure modified from Salvatelli et al. (*in revision*).

SM2 (Text):

Core B-14:

B-14 contained 3 homogeneous deposits identified as slumps (homogeneous deposits II, III and IV in SM1). They have been removed from the record in the present work as they represent instantaneous depositions from upslope. The subsampling in core B-14 was done in stratigraphic intervals (see Salvattecchi et al., 2012 for details), with a mean interval thickness of 0.46 cm.

The chronology for the most recent part of B-14 (last ~150 years) was obtained from downcore profiles of ^{241}Am and excess ^{210}Pb . The older part of B-14, which corresponds to the period below a sedimentary shift where large change in sediment density and several proxies of oxygenation and productivity occurred (Gutierrez et al., 2009), was dated using the sedimentation rates obtained from bulk organic sedimentary carbon of a nearby core B-6. A new chronological model constructed, using the ^{14}C data of Gutierrez et al. (2009) and eliminating the sedimentary sequences identified as slumps in B-6, yields a sedimentation rate of 0.07 cm.y^{-1} (Salvattecchi et al. *in revision*). The sedimentation rates of core B-6 below the sedimentary shift can be used in core B-14 because both cores present similar laminae sequences and the laminae thickness are almost identical (Salvattecchi et al., *in revision*). A cumulative mass-depth profile was used for the $^{210}\text{Pb}_{\text{ex}}$ and ^{14}C profiles due to important changes in sediment density that could give erroneous age estimations. The Dry Bulk Density (DBD) of core B-14 was taken from Salvattecchi et al. (2012), but these values were corrected by sea salt content.

Core G-10:

The laminated section of core G-10 used in the present work is located between 18 and 82 cm depth. Below this section there is a ~35 cm thick slump with laminae reworking (e.g. bands perpendicular to the sedimentation plane). In order to date the core, 32 radiocarbon ages from bulk de-carbonated organic sedimentary carbon were obtained in core G-10, and 7 samples that were taken between 18 and 82 cm depth were used to construct an age model. The conventional radiocarbon ages were calibrated

taking into account global and local reservoir (ΔR) effects using the program Calib 6.1 (Stuiver and Reimer, 1993). The ΔR to calibrate the ^{14}C ages was estimated to be 367 ± 40 years and was calculated for the period between the base of the core B-14 and the last ^{210}Pb -derived age (see also Gutierrez et al., 2009 and Salvattecchi et al., *in revision*). The age model was based on cumulative mass-depth due to important changes in sediment density. The subsampling in core G-10 was done at regular intervals of 1-cm thickness.

Assembled record and core chronologies:

In order to establish the connection between G-10 with B-14 and develop a continuous and reliable record, we performed a laminae cross-correlation between G-10 and the 8 cores retrieved off Pisco that are well cross-correlated (SM1). The first diatom band of the laminated sequence of G-10 (below the homogeneous deposit V) was cross-correlated with the base of the sediment sequence “T” (SM1). Additional support for the fact that this diatom band is contemporaneous in both cores came from similar conventional ^{14}C ages, in core G-10 the age of this band is 1235 ± 30 yr BP while in core B-6 is 1215 ± 30 yr BP. Moreover there is a major slump above the sequence “T” that can be observed in G-10 and several other cores in the area, confirming the tie point of core G-10 with the other records. Consequently, the laminated sequences at the base of core B-14 were deposited just after the first diatom band in core G-10 (~89 cm depth SM1), because the laminated sequences in the base of core B-14 were deposited after the slump V.

The assembled record shows that the sediment structures corresponding to the periods of interest (RWP, DACP, MCA, LIA and CWP) are mainly composed by undisturbed laminated sediments (SM1). The assembled sediment record starts with a homogeneous sediment sequence (SM1). Above this homogeneous deposit an interval containing laminated sequences, which corresponds to the DACP, can be observed up to ~125 cm depth, where another homogeneous deposit is located until ~112 cm depth (SM1). This last homogeneous deposit contains part of the MCA period. The remaining part of the MCA (from ~112 to ~94 cm depth) shows millimeter-scale laminae. The

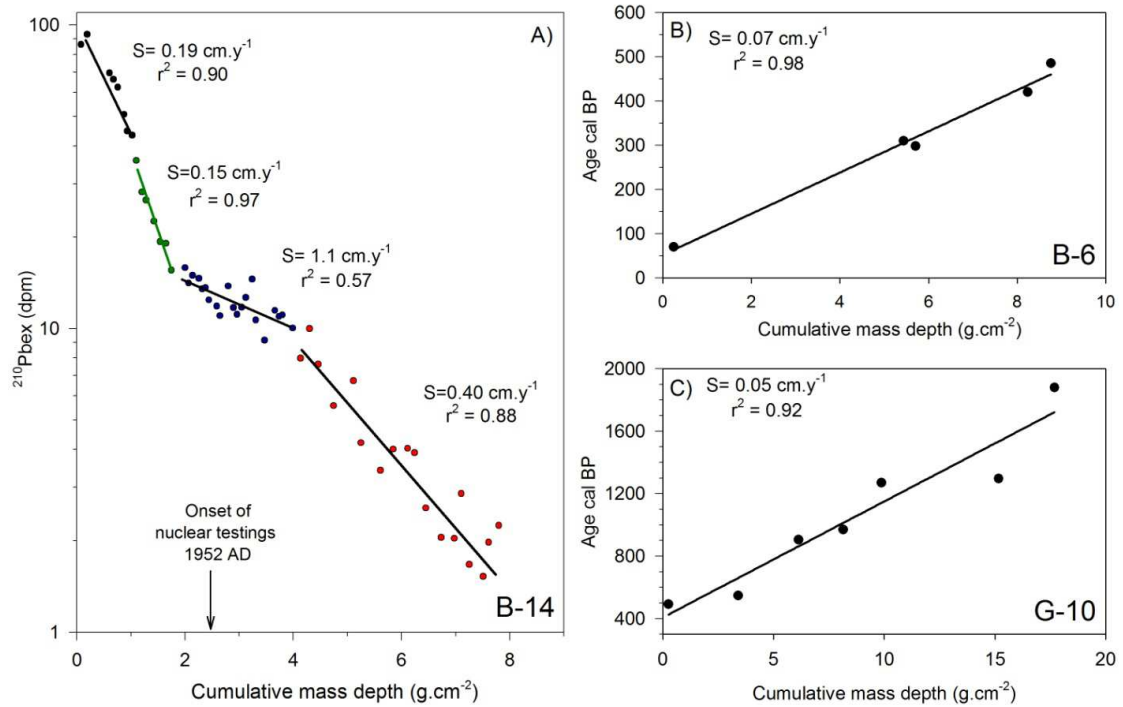
sediment sequences associated with the LIA period show the finest laminated sequences in the entire record. The transition between the LIA and the CWP shows thick diatom bands interspersed with laminated sequences. The CWP shows laminated sediments from ~40 cm to ~23 cm and then from ~4 to the top. The homogeneous section from ~23 to 4 cm depth (SM1) was probably caused by bioturbation or by rapid sedimentation event since the $^{210}\text{Pb}_{\text{ex}}$ profile is relatively constant in this part of the record (Salvatteci et al., *in revision*). An angular unconformity can be observed in core B-14 at ~4 cm depth (SM1). Finally, there is a major change in density at ~62.5 cm depth (SM1) which coincides with a change in sediment density previously reported in a nearby core (Sifeddine et al., 2008; Gutierrez et al., 2009). Based on the sedimentological description and given that we couldn't identify the origin of the two homogeneous deposits (bioturbation or slump) in core G-10 we didn't develop any proxy in these sequences to avoid uncertainty in the data set.

The $^{210}\text{Pb}_{\text{ex}}$ cumulative mass depth profile shows four distinct sections with different sedimentation rates (SM3A). The first section ranges from the top to the angular unconformity located at ~4.3 cm with a sedimentation rate of 0.18 cm.y^{-1} ; the second ranges from 4.3 to 8.5 cm with a sedimentation rate of 0.15 cm.y^{-1} ; the third extends from 8.5 to 23.2 cm with a high sedimentation rate of 1.1 cm.y^{-1} and the last section ranges from 23.2 to 46.6 cm and has a sedimentation rate of 0.40 cm.y^{-1} . The chronological model was adjusted using the ^{241}Am profile by assigning the date 1952AD to 15.6 cm depth. The sedimentation rate for the fourth section (0.402 cm.y^{-1}) was extrapolated up to 62.5 cm where the sedimentary shift is located. The angular unconformity at ~4 cm in core B-14 was identified as a hiatus of ~4 years that occurred approximately at ~1982 AD.

The sedimentation rates during the RWP, DACP, MCA and LIA estimated using ^{14}C ages are considerably lower in comparison with the sedimentation rates of the last 150 years. SM3B shows the cumulative mass depth vs. age cal BP in core B-6, showing the sedimentation rate used to determine the B-14 ages prior to the sedimentary shift (yellow lines in SM1). The sedimentation rate for the pre-shift period in core B-6 was

estimated to be 0.07 cm.y^{-1} (Fig. SM3B). In core G-10 the cumulative mass depth vs. age cal BP yields a sedimentation rate of 0.05 cm.y^{-1} (SM3C). The differences in the sedimentation rates (between periods) and the different subsampling thickness (between cores) indicate that the average time span of each sampled interval during the RWP, DACP, MCA, LIA and CWP is 21.9, 21.9, 7.5 and 1.1 years respectively. Consequently, the proxies obtained in the samples corresponding to the LIA and CWP periods were lumped in intervals of approximately 20 years, and then the results are presented as standardized values (value-average/sd).

SM3 (Figure):



SM3: Cumulative mass-depth age models showing the sedimentation rates used in the present work. A) Core B-14, showing 4 distinct sedimentation rates. B) Core B-6, ^{14}C data taken from Gutierrez et al. (2009) and sedimentation rate obtained from Salvattecchi et al. (*in revision*). C) Sedimentation rates in core G-10. The local reservoir (ΔR) used to calibrate the ^{14}C ages in cores B-6 and G-10 was 367 ± 40 years, see Gutierrez et al. (2009) and Salvattecchi et al. (*in revision*).

SM4 (Text):

Analytical procedures of elements serving as proxies

Major elements (Al and Ti) and trace elements (Mo, V, Re, Cd, Ni and Cu) concentrations were analyzed by ICP-MS (Ultramass Varian) after hot-plate acid digestion in Polytetrafluoroethylene (PTFE) vessels. The acids employed (HF, HNO₃ and HClO₄) eliminated OM and removed silicates (Jarvis et al., 1992). The methodology for the sample preparation is based on Jarvis et al. (1992) and briefly summarized here. First, 25 mg of powdered sample were weighed in a high-precision microbalance and placed into the PTFE vessels. Then, 2 ml of HNO₃ (65%) and 2 ml of HF (40%) were added to the samples. The vessels were closed and immersed in an ultrasonic bath for 10 minutes to facilitate the oxidation of OM. After 2 days, the closed vessels were placed on a hot plate (150°C) for three hours, and then the samples were removed from the hot plate to cool down. As soon as they were cool enough, the open samples were placed again on a hot plate (150°C) to let all the acid evaporate (duration ~5 hours). Then, 2 ml of HF (40%) and 1 ml of HClO₄ (70-72%) were added to the sample and the tubes were placed on a hot plate (150°C) for 10 hours in order to let all the acid evaporate. When the evaporation was completed, 2 ml HNO₃ (65%) were added to the samples and the tubes were placed again on the hot plate to evaporate the remaining acid (2-3 hours). This last procedure was repeated twice. Finally, the samples were placed into larger plastic tubes with the aid of a funnel and HNO₃ (2%). The samples were then analyzed in an ICP-MS and the accuracy of the trace elements concentration measurements was determined through comparison with international standards. The measurement precision was determined by performing duplicate analyses. The average values of replicate digestions were well within the recommended ranges with relative standard deviations (RSD) being <1% for Al, Ti, Mo, V, Ni and Cu, and <2.5% for Re (n = 229).

The total metal concentrations measured contain a detrital background and an authigenic metal concentration (i.e. the part in excess of the detrital background; Böning et al., 2004; Tribovillard et al., 2006; Scholz et al., 2011). Given that the trace elements may present in some cases a strong detrital fraction, we focus on the authigenic trace

element content. The chemical composition of andesite is an appropriate representation of the detrital background of the sediments on the Peruvian margin as proposed by Böning et al. (2004). Thus, we used the element contents of andesite to obtain the authigenic concentration of each trace element. These contents were obtained from the GEOROC database (Sarbas and Nohl, 2009) taking into account the elements concentrations in andesite from whole rocks from the central Andean volcanic zone in Peru (SM5). The detrital metal fraction was calculated following Tribovillard et al. (2006): $X_{\text{detrital}} = (X/Al)_{\text{andesite}} * Al_{\text{sample}}$. Consequently the authigenic fraction of element X in a sample was calculated as $X_{\text{total}} - X_{\text{detrital}}$. The authigenic (or non-lithogenic) fraction is mainly enriched by post-depositional redox reactions (especially in suboxic environments) and each element exhibits different sensitivities to redox conditions along an oxic to sulfidic gradient. However not all the authigenic fraction is produced only by post-depositional reactions because some metal fraction present above the background lithogenic concentrations is also due to the flux of metals associated with settling biological material (Nameroff et al., 2004; Tribovillard et al., 2006). We calculated the enrichment factor of the elements to determine if they are depleted or enriched relative to andesite. The enrichment factors were calculated using the following formula according to Tribovillard et al. (2006): $EF_{\text{element x}} = (X/Al)_{\text{sample}} / (X/Al)_{\text{andesite}}$. If EF_x is greater (lower) than 1, then the element X is enriched (depleted) relative to average shales.

The biogenic silica was quantified by Fourier transformed infrared spectrometry (FTIR) analyses (Bertaux et al. 1998). The sample preparation for FTIR analysis is described by Bertaux et al. (1998) and is briefly summarized here. Given that a particle size of less than 2 μm is required to avoid excessive scattering of infrared (IR) radiation, approximately 15 mg of dry pre-powdered sample were mechanically ground with small agate balls in an agate vial under acetone and in a cooling chamber for 90 minutes. Then, the solution containing the powdered sample and the acetone was poured onto a watch glass to let the acetone evaporate. After that, 2.5 mg of dry pre-powdered sample were weighed in a high-precision microbalance and 997.5 mg of KBr was added to the sample. Then, the powder containing the sample and KBr was mixed by hand in an agate mortar for 10 minutes and 300 mg of this powder was used to prepare a 13 mm diameter disc by

pressing the mixture in a vacuum die with up to 8 tons.cm⁻² of compression. Finally, in order to acquire the IR spectra, the discs were placed into a Perkin-Elmer FT 16 PC spectrometer in the 4000–250 cm⁻¹ energy range with a 2 cm⁻¹ resolution. In order to quantify the % of biogenic silica from the IR spectra the spectral-energy range between 1315 and 315 cm⁻¹ was chosen for calculation because this region yields many absorption features that are relevant for distinguishing the biogenic silica in the mixture. The % of amorphous silica obtained from the FTIR analysis also incorporates other types of amorphous silica (e.g., volcanic ashes) but their concentrations are too low in comparison with the vast abundance of diatoms valves off Peru, thus we consider that the % of amorphous silica obtained through the FTIR analysis reflects principally the % of biogenic silica.

The quantification of organic matter was done using Rock-Eval 6 that permits evaluation of the evolution of organic compounds during programmed pyrolysis (Lafargue et al. 1998). During the programmed pyrolysis several parameters are used in order to quantify and characterize the organic matter: S1, S2 and S3. S1 (mg HC/g rock) corresponds to the quantity of hydrocarbons (HC) released during the isothermal temperature step at 300°C and represents the thermo-vaporized free hydrocarbons contained in the rock (Behar et al. 2001). S2 (mg HC/g rock) corresponds to the quantity of HC released between 300 and 650°C and represents the HC resulting from the cracking of sedimentary organic matter (Behar et al. 2001). Finally, S3 (mg CO₂/g rock) represents milligrams of carbon dioxide generated from a gram of sample during temperature programming up to 390°C (Lafargue et al. 1998; Behar et al., 2001; Peters et al. 2005). Total Organic Carbon (TOC) is determined by summing the pyrolysable organic carbon (obtained from the S1, S2 and S3) and the residual organic carbon (Behar et al. 2001). TOC reflects the quantity of OM present in the sediment and can be used to infer past export production.

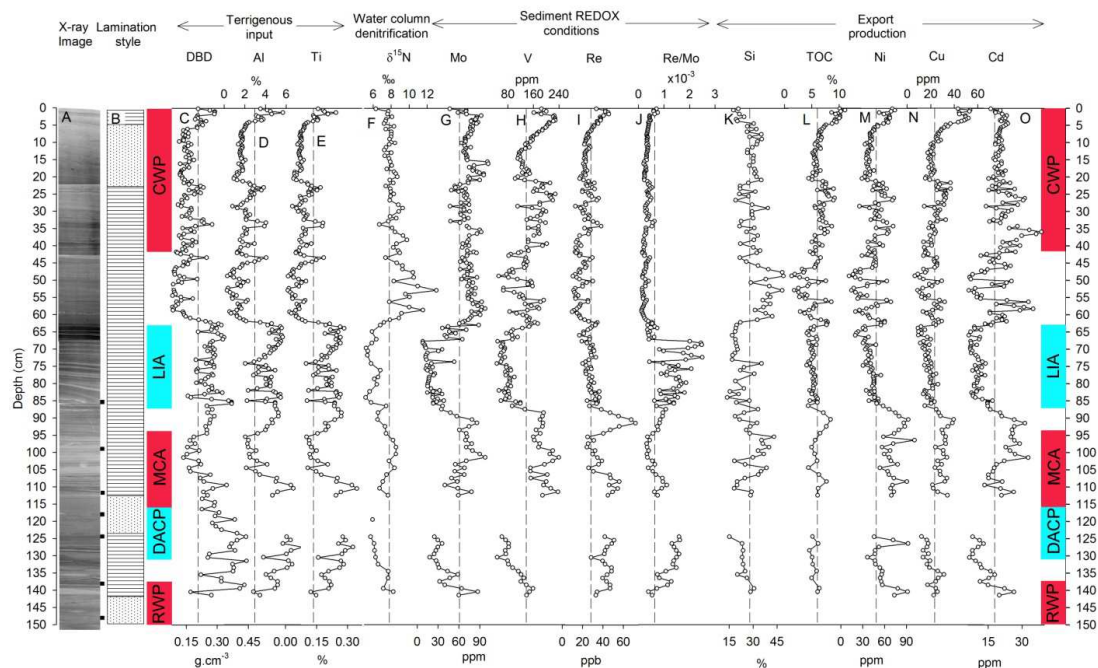
The water column denitrification was inferred through $\delta^{15}\text{N}$ in sedimentary organic matter and the analyses were performed in two different laboratories. $\delta^{15}\text{N}$ analyses for core B-14 were done in the ALYSEES at Bondy, France and were measured on a continuous-flow gas-ratio mass spectrometer. Standardization was based on a

laboratory standard Tyrosine and Urea. $\delta^{15}\text{N}$ analyses for core G-10 were done in the department of Geosciences of the University of Arizona and were measured on a continuous-flow gas-ratio mass spectrometer (Finnigan Delta PlusXL) coupled to an elemental analyzer (Costech). Standardization was based on laboratory standard acetanilide and the precision was better than ± 0.2 (1s).

SM5 (Table): Average (\pm sd) concentration and Metal/Al for Andesite in whole rocks from the central Andean volcanic zone in Peru taken from the GEOROC database (Sarbas and Nohl, 2009) and in marine sediments from the present study. Re concentration and Re/Al from andesite taken from Alves et al. (2002).

Metal	Element/Al				
	Andesite		Present study		
	average	sd	average	sd	
V/Al ($\times 10^{-3}$)	1.4	\pm 0.6	7.7	\pm 3.8	
Cu/Al ($\times 10^{-4}$)	4.4	\pm 3.3	14.7	\pm 5.4	
Ni/Al ($\times 10^{-4}$)	2.6	\pm 2.8	22.6	\pm 8.6	
Mo/Al ($\times 10^{-5}$)	2.5	\pm 1.9	337.9	\pm 340.8	
Cd/Al ($\times 10^{-6}$)	2.6	\pm 2.4	861.2	\pm 560.3	
Re/Al ($\times 10^{-9}$)	1.9		1121.2	\pm 459.0	

SM 6 (Figure):



SM6. X-ray images, lamination style, time periods of interest, and proxies evaluated in the present study. A) Positive X-ray image of cores B-14 and G-10 (from 87 cm to the bottom); the small boxes at the right side of the X-ray image indicate the position of the samples that were dated by ^{14}C in core G-10. B). Simplified lithology, the areas with horizontal lines represent finely laminated sediments and the dotted areas represent mixed sediments or more homogeneous material. C) Dry Bulk Density (DBD), data of core B-14 taken from Salvatelli et al. (2012) corrected by sea salt content. D) Al (%), proxy for terrigenous input. E) Ti (%) proxy for terrigenous input. F) $\delta^{15}\text{N}$ (‰) proxy for water column denitrification. G), H) and I) Authigenic molybdenum (Mo, ppm), authigenic vanadium (V, ppm) and authigenic rhenium (Re, ppb) proxies for sediment redox conditions. J) Re/Mo ($\times 10^{-3}$), proxy to differentiate anoxic vs. suboxic conditions. K) Biogenic Silica (Si%), proxy of diatom production. L), M), N) and O) Total organic carbon (TOC, %), authigenic nickel (Ni, ppm), authigenic copper (Cu, ppm) and authigenic cadmium (Cd, ppm), export production proxies. The horizontal dashed lines indicate the average of each proxy. The colored boxes at the right and left side of the figure indicate the Roman Warm Period (RWP), the Dark Ages Cold Period (DACP), the Medieval Climate Anomaly (MCA), the Little Ice Age (LIA) and the Current Warm Period (CWP) according to the age model presented in SM3. Note that in this figure, Cd is presented as an export production proxy while in Figures 2 this trace metal is used to reconstruct sediment redox conditions, see text in the manuscript for more information.

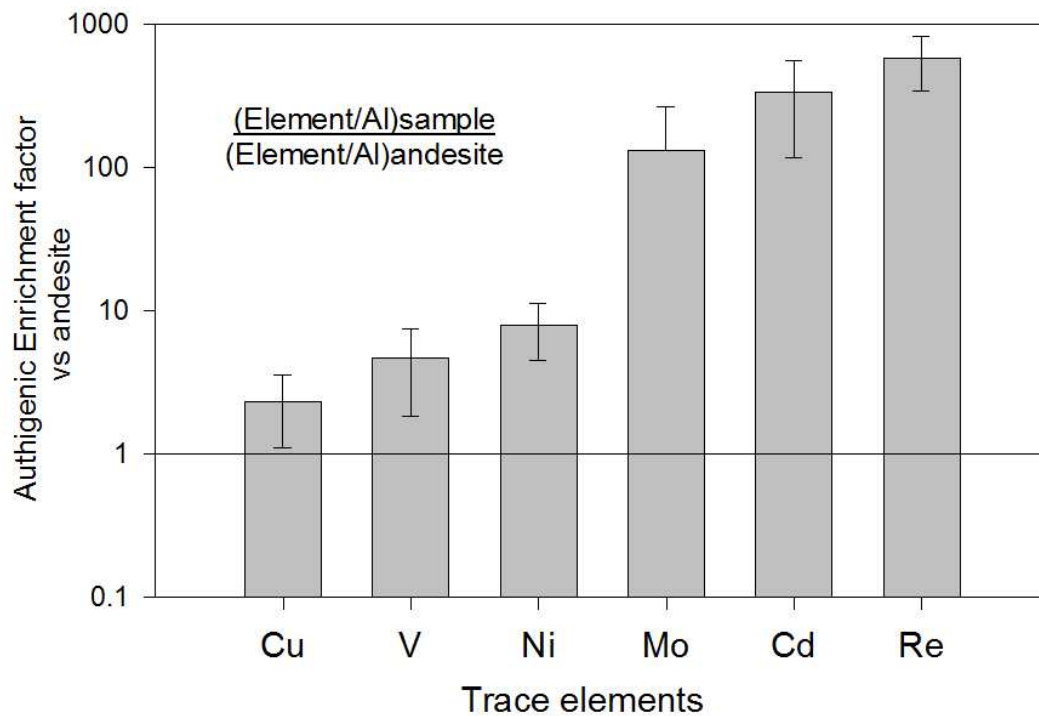
SM7 (Table): Correlation matrix based on the Pearson correlation coefficients (r values) for Al and Ti (n=229), authigenic metal concentrations (n=229); biogenic silica (n=127); total organic carbon (TOC, n=203) and $\delta^{15}\text{N}$ (n=105) in cores B-14 and G-10. Data from SM6. Underlined values indicate significance after correcting for multiple comparisons ($p < 0.004$). Cadmium is considered as an export production proxy in this Table, but given its high relationship with the other sediment redox conditions proxies, is used from hereon as a proxy for oxygen availability in the sediments rather than productivity. The probability level was corrected for multiple comparisons by dividing the probability level α ($p < 0.05$) by the number of test (12) performed (Glantz 2002). The values in parentheses indicate that were derived from two categories that share the same data (Mo, Re and Re/Mo).

		DBD (g.cm^{-3})	Al (%)	Ti (%)	Mo (ppm)	V (ppm)	Re (ppb)	Re/Mo	$\delta^{15}\text{N}$ (‰)	Biogenic silica (%)	TOC (%)	Ni (ppm)	Cu (ppm)	Cd (ppm)
Terrigenous input	DBD (g.cm^{-3})	1												
	Al (%)	<u>0.82</u>	1											
	Ti (%)	<u>0.80</u>	<u>0.99</u>	1										
Sediment REDOX conditions	Mo (ppm)	<u>-0.64</u>	<u>-0.67</u>	<u>-0.69</u>	1									
	V (ppm)	<u>-0.25</u>	-0.14	-0.16	<u>0.61</u>	1								
	Re (ppb)	<u>0.62</u>	<u>0.72</u>	<u>0.71</u>	<u>-0.23</u>	<u>0.28</u>	1							
	Re/Mo	<u>0.63</u>	<u>0.71</u>	<u>0.73</u>	<u>(-0.88)</u>	<u>-0.49</u>	<u>(-0.41)</u>	1						
OMZ intensity	$\delta^{15}\text{N}$ (‰)	<u>-0.69</u>	<u>-0.75</u>	<u>-0.75</u>	<u>0.68</u>	0.22	<u>-0.55</u>	<u>-0.72</u>	1					
Export production	Biogenic silica (%)	<u>-0.58</u>	<u>-0.73</u>	<u>-0.71</u>	<u>0.50</u>	0.01	<u>-0.48</u>	<u>-0.58</u>	<u>0.75</u>	1				
	TOC (%)	0.13	<u>0.21</u>	0.16	<u>0.24</u>	<u>0.75</u>	<u>0.57</u>	-0.09	-0.28	<u>-0.46</u>	1			
	Ni (ppm)	<u>0.28</u>	<u>0.39</u>	<u>0.38</u>	0.08	<u>0.60</u>	<u>0.75</u>	0.08	<u>-0.28</u>	-0.25	<u>0.74</u>	1		
	Cu (ppm)	-0.01	0.04	0.01	<u>0.35</u>	<u>0.75</u>	<u>0.47</u>	<u>-0.19</u>	-0.05	-0.13	<u>0.87</u>	<u>0.67</u>	1	
	Cd (ppm)	<u>-0.40</u>	<u>-0.37</u>	<u>-0.39</u>	<u>0.70</u>	<u>0.76</u>	0.08	<u>-0.54</u>	<u>0.37</u>	0.19	<u>0.57</u>	<u>0.52</u>	<u>0.56</u>	1

SM 8 (Table): Correlation matrix based on the Pearson correlation coefficients (r values) for metal/Al ratios (n=229); biogenic silica (n=127); total organic carbon (TOC, n=203) and $\delta^{15}\text{N}$ (n=105) in cores B-14 and G-10. Underlined values indicate significance after correcting for multiple comparisons ($p < 0.056$). Cadmium is considered as an export production proxy in this Table, but given its high relationship with the other sediment redox conditions proxies, is used hereafter as a proxy for oxygenation rather than productivity. The probability level was corrected for multiple comparisons by dividing the probability level α ($p < 0.05$) by the number of test (9) performed (Glantz 2002).

	Mo/Al	V/Al	Re/Al	Re/Mo	$\delta^{15}\text{N}$ (‰)	Biogenic silica (%)	TOC (%)	Ni/Al	Cu/Al	Cd/Al
Sediment REDOX conditions	Mo/Al	1								
	V/Al	<u>0.87</u>	1							
	Re/Al	<u>0.89</u>	<u>0.84</u>	1						
	Re/Mo	<u>-0.56</u>	<u>-0.73</u>	<u>-0.54</u>	1					
OMZ intensity	$\delta^{15}\text{N}$ (‰)	<u>0.79</u>	<u>0.84</u>	<u>0.65</u>	<u>-0.72</u>	1				
Export production	Biogenic silica (%)	<u>0.69</u>	<u>0.73</u>	<u>0.66</u>	<u>-0.58</u>	<u>0.75</u>	1			
	TOC (%)	<u>-0.43</u>	-0.16	<u>-0.22</u>	-0.09	<u>-0.28</u>	<u>-0.46</u>	1		
	Ni/Al	<u>0.76</u>	<u>0.88</u>	<u>0.80</u>	<u>-0.67</u>	<u>0.74</u>	<u>0.74</u>	-0.06	1	
	Cu/Al	<u>0.81</u>	<u>0.92</u>	<u>0.84</u>	<u>-0.69</u>	<u>0.76</u>	<u>0.70</u>	-0.02	<u>0.87</u>	1
	Cd/Al	<u>0.78</u>	<u>0.90</u>	<u>0.73</u>	<u>-0.70</u>	<u>0.80</u>	<u>0.70</u>	-0.16	<u>0.88</u>	<u>0.88</u>

SM9 (Figure):



SM9. Enrichment factors for several trace elements vs. average andesitic composition and standard deviation (sd). The element/Al from andesite were obtained from the GEOROC database (Sarbas and Nohl 2009) taking into account the element concentrations in andesite from whole rocks from the central Andean volcanic zone in Peru. Andesite Re/Al ratio was taken from Alves et al. (2002). All data available from cores B-14 and G-10 were used to calculate the averages. The Mo –sd is off scale. Re, Cd and Mo exhibited the highest enrichments factors (average ±sd): 578 ± 236 ; 334 ± 218 and 131 ± 134 ; Ni and V show a moderate enrichment of 7.9 ± 3.4 and 4.7 ± 2.8 respectively. Finally, Cu showed the lowest enrichment factor: 2.3 ± 1.2 .

SM10 (Text):

Correlation among proxies and data presentation

The downcore profiles of all the proxies evaluated in this study are plotted in SM6, showing that the proxies that represent the same process are highly correlated with exception of Cd that seems to represent sediment redox conditions instead of export production (SM6 and SM7). The terrestrial runoff proxies (Al and Ti) show similar downcore variability and are highly correlated (SM6, SM7). Al and Ti% follow the same downcore changes observed in the DBD values (SM6C, D and E) and also show a strong correlation with the DBD values (SM7). Additionally, there is a strong negative correlation of the biogenic silica contents with DBD, Al and Ti (SM7; -0.63, -0.75 and -0.72, $n = 119$, $p < 0.001$). These results are expected because Al and Ti% represent the detrital fraction, which is denser than the other components of the sedimentary matrix (i.e. OM, biogenic silica and calcium carbonate).

The relationships among the proxies for sediment redox conditions (Mo, V, Re and Re/Mo), and their relationships with the water column denitrification ($\delta^{15}\text{N}$) also show an expected pattern. The three sediment redox conditions proxies (Mo, V and Re) show an expected relationship based on their sensitivity to oxygen levels in the sediments. Mo and V show the strongest correlation (SM7; 0.61), because both of them accumulate under anoxic conditions with H_2S presence (Scholz et al. 2011). However, their relationship is not so high probably due to the high frequency variability in the V profile during the LIA-CWP transition not observed in the Mo profile. Mo and Re show a negative relationship (SM7; -0.23) as expected due to their different sensitivity to H_2S availability. The $\delta^{15}\text{N}$ profile shows a coherent pattern with Mo and Re/Mo (SM6), exhibiting high and significant correlations with Mo and with Re/Mo (SM7; 0.68 and -0.72 respectively).

The proxies for export production show some similarities and differences that can be used to interpret changes in productivity during the last 2 millennia. Biogenic silica contents show negative correlations with the other export production proxies indicating that the overall export production (i.e. from higher trophic levels) is not a simply function

of siliceous productivity. The biogenic silica shows negative relationships with TOC, Ni and Cu (SM7; -0.46, -0.25 and -0.13). Higher biogenic silica contents are associated with visible diatoms bands in the X-ray images, which are present during the LIA-CWP transition and during some periods within the MCA and CWP (SM6). There are some differences among the overall export production proxies that suggest that TOC, Ni and Cu are better indicators than Cd. First, Ni and Cu show higher correlation (SM7; 0.67) than Ni with Cd (Table 2, 0.52) or Cu with Cd (SM7; $r = 0.56$). Second, the correlations of Cd with the proxies for sediment redox conditions (Mo and V; SM7; 0.70 and 0.76 respectively) are higher than those for export production. Third, the correlations between Ni and Cu with TOC (SM7; 0.74 and 0.87) are higher than that of Cd and TOC (SM7; 0.57). Finally, the increment in TOC in the last ~50 years is replicated by the Ni and Cu profiles but not by the Cd profile (SM6 L, M, N and O). The similarity between the Ni, Cu and TOC profiles is likely due to the fact that both metals are exported to the sediments in association with organometallic complexes, while the differences with the Cd profile may probably arise from post-depositional processes (Tribovillard et al., 2006). These results suggest that Ni and Cu are better proxies to OM flux than Cd because the export production signal of Cd may be obscured by metal enrichment in the water-sediment interface during anoxic conditions. Therefore, Cd is used from here onwards as a proxy for redox conditions and not for export production.

Normalization of trace elements concentrations through division by Al as well as the calculation of fluxes (Metal concentration x sedimentation rates x DBD) through the use of the sedimentation rates obtained from age models, are common practices. However, in the present dataset, the normalization procedure increased, decreased, or even changed the sign of the correlations between unmodified variables. Authigenic trace element concentrations in the Pisco cores that were not correlated, like Ni with Mo (SM7, 0.08) or Re with Cd (SM7, 0.08) show a strong shared variability when the data are normalized by Al (SM8, Ni/Al with Mo/Al: 0.78 and Re/Al with Cd/Al: 0.73). Additionally, the strong correlations of the authigenic paleoproductivity proxies with TOC disappeared when the trace elements were normalized (SM7 and SM8). For example the correlations of authigenic Ni and Cu contents with TOC were 0.74 and 0.87

respectively, while the correlations of normalized Ni and Cu with TOC were -0.06 and -0.02 (SM7). The normalization problems may arise when the coefficient of variation (standard deviation divided by the mean) of Al concentrations is large compared to the coefficients of variation of the other trace elements. In the present work the coefficient of variation of Al (0.53) was relatively high in comparison with Ni (0.33), Cu (0.37), Cd (0.38), Mo (0.39), V (0.35), and Re (0.37). Thus, the changes observed in the normalized variables are likely due to the relatively high coefficient of variation of Al. These observations indicate that the normalization by Al should be avoided in the data set present on this study. Nonetheless, the average enrichment factor of each element in all the record was calculated to determine which elements exhibit the highest enrichments relative to andesite (SM9). Re, Cd and Mo exhibited the highest enrichments factors (average \pm sd): 578 ± 236 ; 334 ± 218 and 131 ± 134 ; Ni and V show a moderate enrichment of 7.9 ± 3.4 and 4.7 ± 2.8 respectively. Finally, Cu showed the lowest enrichment factor: 2.3 ± 1.2 . The high and moderate enrichment factors of Re, Cd, Mo, Ni, and V support their use as paleoredox or paleoproductivity proxies.

Another possibility to present the data set is as fluxes (Metal concentration \times sedimentation rates \times DBD) through the use of the sedimentation rates obtained from the age models (SM3). This approach should also be taken with caution since the fluxes are highly sensitive to the sedimentation rates, even though if a careful age model was constructed as in the present work (Van der Weijden 2002). As also observed in the case of the Al normalization, the large variations in the sedimentation rates (SM3) produce distorted correlations between elements (data not shown). Consequently, we present the authigenic concentrations of the trace elements instead of the Al normalization or metal accumulation rates. In the following sections, the proxies shown in Supplementary Material 6 are plotted versus a time scale, and the samples corresponding to the LIA and CWP are lumped into coarser samples in order to obtain the same temporal resolution in all the record.

REFERENCE LIST (SUPPLEMENTARY MATERIAL):

- Alves, S., P. Schiano, F. Capmas, and C. J. Allègre. 2002. Osmium isotope binary mixing arrays in arc volcanism. *Earth and Planetary Science Letters* 198(3-4):355-369.
- Behar, F., V. Beaumont, and H. L. D. B. Penteadó. 2001. Rock-Eval 6 technology: performances and developments. *Oil & Gas Science and Technology - Rev. IFP* 56(2):111-134.
- Bertaux, J., F. Frohlich, and P. Idefonse. 1998. Multicomponent analysis of FTIR spectra: Quantification of amorphous and crystallized mineral phases in synthetic and natural sediments. *Journal of Sedimentary Research* 68:440-447.
- Böning, P., H. J. Brumsack, E. Bottcher, B. Schnetger, C. Kriete, J. Kallmeyer, and S. L. Borchers. 2004. Geochemistry of Peruvian near-surface sediments. *Geochimica et Cosmochimica Acta* 68(21):4429-4451.
- Glantz, S. A. 2002. *Primer of Biostatistics*. McGraw-Hill.
- Gutierrez, D., A. Sifeddine, D. B. Field, L. Ortlieb, G. Vargas, F. Chavez, F. Velazco, V. Ferreira, P. Tapia, R. Salvattecí, H. Boucher, M. C. Morales, J. Valdes, J. L. Reyss, A. Campusano, M. Boussafir, M. Mandeng-Yogo, M. Garcia, and T. Baumgartner. 2009. Rapid reorganization in ocean biogeochemistry off Peru towards the end of the Little Ice Age. *Biogeosciences* 6:835-848.
- Jarvis, K. E., A. L. Gray, and R. S. Houk. 1992. *Handbook of Inductively Coupled Plasma Mass Spectrometry*. Blackie Academic & Professional, an imprint of Chapman & Hall, Wester Cleddens Road, Bishopbriggs, Glasgow, London Glasgow New York Tokyo Melbourne Madras.
- Lafargue, E., J. Espitalié, F. Marquis, and D. Pillot. 1998. Rock-Eval 6 applications in hydrocarbon exploration, production and in soil contaminations studies. *Oil & Gas Science and Technology - Rev. IFP* 53(4):421-437.
- Nameroff, T. J., S. E. Calvert, and J. W. Murray. 2004. Glacial-interglacial variability in the eastern tropical North Pacific oxygen minimum zone recorded by redox-sensitive trace metals. *Paleoceanography* 19:PA1010.
- Peters, K. E., C. C. Walters, and J. M. Moldowan. 2005. *The Biomarker Guide*. Cambridge University Press.

- Sarbas, B., and U. Nohl. 2009. The GEOROC database - a decade of "online geochemistry". *Geochimica et Cosmochimica Acta* 73(A1158).
- Salvatteci, R., D. B. Field, T. Baumgartner, V. Ferreira, and D. Gutierrez. 2012. Evaluating fish scale preservation in sediment records from the oxygen minimum zone off Peru. *Paleobiology* 38(1):766-792.
- Salvatteci, R., D. Field, A. Sifeddine, L. Ortlieb, V. Ferreira, T. Baumgartner, S. Caquineau, F. Velazco, J. L. Reyss, J. A. Sanchez-Cabeza, and D. Gutierrez. (in revision). Cross-stratigraphies from a seismically active mud lens off Peru indicate horizontal extensions of laminae, missing sequences, and a need for multiple cores for high resolution records. *Marine Geology*.
- Scholz, F., C. Hensen, A. Noffke, A. Rohde, V. Liebetrau, and K. Wallmann. 2011. Early diagenesis of redox-sensitive trace metals in the Peru upwelling area – response to ENSO-related oxygen fluctuations in the water column. *Geochimica et Cosmochimica Acta* 75:7257-7276.
- Stuiver, M., and P. J. Reimer. 1993. Extended ^{14}C database and revised CALIB radiocarbon calibration program. *Radiocarbon* 35:215-230.
- Tribovillard, N., T. J. Algeo, T. Lyons, and A. Riboulleau. 2006. Trace metals as paleoredox and paleoproductivity proxies: An update. *Chemical Geology* 232:12-32.
- Van der Weijden, C. H. 2002. Pitfalls of normalization of marine geochemical data using a common divisor. *Marine Geology* 184:167-187.